JGR Atmospheres

RESEARCH ARTICLE
10.1029/2025JD044703

Construction of Albedo Schemes for the Typical Underlying Surface on the Tibetan Plateau Under Snow Free Conditions

Huan Wang[1], Anning Huang[1], Chunlei Gu[1], Xinsheng Zhu[2], Lijuan Wen[3], and Jiangxin Luo[1,4]

[1]School of Atmospheric Sciences, Nanjing University, Nanjing, China, [2]Nanjing Institute of Environmental Sciences, Ministry of Ecology and Environment of the People's Republic of China, Nanjing, China, [3]Northwest Institute of Eco-Environment and Resources State Key Laboratory of Frozen Soil Engineering, Lanzhou, China, [4]Southwest Electric Power Design Institute Co., Ltd., China Power Engineering Consulting Group, Chengdu, China

Key Points:

- The albedo schemes suitable for the grassland and bare land on the Tibetan Plateau have been constructed respectively
- Adopting the newly developed albedo schemes in the CLM5 model can obviously improve the albedo simulations on the Tibetan Plateau
- The improved albedo simulation further clearly reduces the biases in the surface thermal condition simulations on the Tibetan Plateau

Correspondence to:
A. Huang and X. Zhu,
anhuang@nju.edu.cn;
zxs_dream@yeah.net

Citation:
Wang, H., Huang, A., Gu, C., Zhu, X., Wen, L., & Luo, J. (2026). Construction of albedo schemes for the typical underlying surface on the Tibetan Plateau under snow free conditions. *Journal of Geophysical Research: Atmospheres*, *131*, e2025JD044703. https://doi.org/10.1029/2025JD044703

Received 25 JUN 2025
Accepted 10 FEB 2026

Author Contributions:
Conceptualization: Anning Huang
Data curation: Huan Wang, Jiangxin Luo
Formal analysis: Huan Wang, Anning Huang, Chunlei Gu, Xinsheng Zhu
Investigation: Huan Wang, Anning Huang, Chunlei Gu, Lijuan Wen
Methodology: Huan Wang, Anning Huang
Resources: Huan Wang, Chunlei Gu, Lijuan Wen, Jiangxin Luo
Software: Huan Wang
Supervision: Anning Huang, Xinsheng Zhu
Validation: Huan Wang, Anning Huang, Chunlei Gu
Visualization: Huan Wang
Writing – original draft: Huan Wang, Anning Huang, Xinsheng Zhu, Jiangxin Luo
Writing – review & editing: Huan Wang, Anning Huang, Chunlei Gu, Xinsheng Zhu, Lijuan Wen

Abstract The surface albedo plays a crucial role in regulating the allocation of solar radiation between the surface and atmosphere over the Tibetan Plateau (TP), and significantly influences the heat transfer from the surface to the overlying atmosphere. This study used field observation data to reveal the key factors affecting the albedo of two typical underlying surfaces (bare land, alpine grassland) under snow free conditions. Results show that the solar elevation angle, soil ice content, soil liquid content, and near canopy surface air relative humidity are the primary determinants of albedo for these typical surfaces. Based on these findings, the albedo schemes suitable for the bare land and alpine grassland on the TP have been constructed by considering more comprehensive affecting factors. Evaluation of single-point simulations at four stations indicates that adopting the new albedo schemes can clearly improve the albedo simulations of Community Land Model version 5 (CLM5) with the root mean square error reduced by ∼10% to ∼60% relative to adopting the original albedo schemes, further leading to the surface net radiation simulations improved and thereafter the warm biases of soil temperature simulations reduced by ∼0.2°C to ∼1°C. Regional simulation verification further confirms that adopting the new albedo schemes in CLM5 can obviously improve the surface net radiation simulations by increasing the albedo simulation accuracy on the TP, thereby mainly reducing the overestimation of surface sensible heat flux and land surface temperature by the original albedo schemes, further resulting in the performance of CLM5 to simulate the TP surface heat conditions enhanced.

Plain Language Summary In addition to snow cover, two typical underlying surfaces (bare land, alpine grassland) are widely distributed on the Tibetan Plateau (TP). In this study, the main factors affecting the albedo of the two typical underlying surfaces on the TP under snow free conditions have been identified based on the field observation data, and two albedo schemes have been developed by considering more comprehensive affecting factors tailored to the TP region with much higher accuracy in simulating the albedos of the two typical underlying surfaces. We further explore to what extent the newly developed albedo schemes affect the performance of the CLM5 model in simulating the surface albedo and thermal conditions on the TP under snow free conditions. The results show that the underestimation of albedo on the TP in the CLM5 model can be obviously reduced by adopting the newly developed albedo schemes, and the overestimation of land surface temperature and sensible heat flux simulations is clearly decreased correspondingly. This study provides a potential way to further improve the simulations of surface thermal conditions on the TP in numerical models.

1. Introduction

The Tibetan Plateau (TP) is characterized by the highest altitude, steepest slope, and largest plateau in the world. Due to its high altitude, low air density, and short path of solar radiation to reach the surface, the TP can receive strong solar radiation, which can also transport a large amount of heat from the surface to the atmosphere. Such strong sensible heat flux transfer from the surface to the atmospheric boundary layer makes it an important external forcing for atmospheric movement in the Northern Hemisphere, not only affecting the climate of the Asian monsoon region but also the climate of the Northern Hemisphere and even the world (Duan et al., 2013; Wu et al., 2007, 2015, 2018; Yimin et al., 2020).

The surface albedo can directly influence the allocation of solar radiation between the surface and the atmosphere. Even a minor change in albedo can significantly affect the radiation energy balance in the Earth's atmosphere system. Previous studies have shown that a 0.01 shift in surface albedo can result in an energy change of 3.4 W/m^2, which is about 1.5–5 times more powerful than carbon dioxide in changing global surface air temperature

(Irvine et al., 2011; Jorgensen et al., 2014; Liang et al., 2010; Sedlar et al., 2011; Wielicki et al., 2005). Changes in the TP surface albedo can alter the heat transfer from the plateau to the atmosphere, the structure of the temperature and pressure fields over the TP, and further affect the intensity and duration of Asian monsoon and precipitation (Cao et al., 2019; Cen et al., 2014; Tang et al., 2023; Zhao et al., 2013). Therefore, improving the simulation accuracy of surface albedo to enhance the simulation of the TP thermal effect in weather and climate models is of great importance.

Snow cover is the most important type of land cover on the TP in cold seasons. Currently, the cold biases in temperature simulations over the TP region are mainly due to the simulation errors of snow cover and albedo in the climate models (Gu et al., 2024; Li et al., 2018; Luo et al., 2025; Wu & Qian, 2003; Zhao & Moore, 2004; Zhou et al., 2023). Many studies have tried to improve the simulation of snow cover distribution in the TP from the perspective of sub-grid terrain and wind-blown snow etc., as well as to improve the simulation of snow albedo from aspects such as new snow albedo and snow melting process (Liu et al., 2021, 2022; Miao et al., 2022; Roesch et al., 2001; Sun et al., 1999; Swenson & Lawrence, 2012; Wang et al., 2020; Xie et al., 2019; Zhao et al., 2007). However, the snow cover in the TP has large seasonal variations. In May, the snow begins to melt, and the proportion of the snow cover area can reach less than 0.1 from June to August (Guo et al., 2016). In addition to snow cover, alpine grassland and bare land are widely distributed in the TP, but the current improvement research on the surface albedo simulation in the TP has rarely focused on these underlying surfaces. The albedo characteristics of these land surface types have significant differences. Systematic improvement of the albedo parameterization schemes of these typical underlying surfaces on the TP can improve the accuracy of the albedo simulation in the plateau region. It is of great significance for further improving the simulations of surface thermal conditions in the plateau region and the climate in East Asia.

The spatio-temporal variability of surface albedo is mainly influenced by the factors such as solar elevation angle, soil moisture, soil color, vegetation coverage and surface roughness, etc. According to previous field observation experiments, it is widely accepted that the albedo of the bare surface decreases exponentially (linearly) with an increase in the sine of the solar elevation angle (soil moisture). For the underlying surface with vegetation coverage, the higher vegetation coverage corresponds to the lower surface albedo and the relative humidity near the canopy surface can also affect the albedo (Bao et al., 2008; Cai et al., 2012; Guan et al., 2009; Liu et al., 2008; Roxy et al., 2010; Sugathan et al., 2014; Tian et al., 2018; Zhang & Huang, 2004; Zheng et al., 2014, 2015). Currently, many studies have improved the parameterization scheme of surface albedo based on the above influencing factors, and shown that the introduction of these factors into albedo parameterization schemes can clearly improve the accuracy of albedo simulations and further improve the simulations of surface energy balance (Kala et al., 2014; Liang et al., 2005; Loarie et al., 2011; Wang et al., 2007; Yang et al., 2008; Zheng et al., 2017). However, the climate environment in the TP region is unique, with seasonal frozen soil widely distributed (Luo et al., 2023). Previous improved schemes for the albedos of bare soil and vegetation underlying surfaces may not be fully applicable in this area.

This study used field observation data and satellite data to reveal the main factors affecting the albedos of the bare land and alpine grassland, which are widely distributed in the TP, and developed two new albedo parameterization schemes suitable for the TP with more comprehensive factors considered and higher simulation accuracy. Finally, these newly developed albedo schemes were introduced into the CLM5 land surface model. Meanwhile, this study systematically explored to what extent the newly developed albedo schemes affect the performance of the CLM5 model in simulating the surface albedo and thermal conditions under snow free conditions on the TP, as well as the possible associated reasons. The findings of this study may provide a potential way to further improve the ability of numerical models in simulating the land-air energy exchange and surface thermal conditions on the TP.

2. Study Area

As shown in Figure 1, the alpine grassland is the dominant land cover type on the eastern TP (accounting for about 50% of the TP area), while the bare land is dominant in most parts of the northwestern TP (accounting for about 40% of the TP area). Due to its special geographical location and high altitude, the TP is often covered with a large amount of snow in cold seasons. The TP is less covered with snow in summer and autumn, and more in winter and spring (Guo et al., 2016). Consistent snow accumulation on the TP occurs from October of the preceding year to April of the subsequent year, and the snow cover fraction begins to decrease after May. Therefore, this study

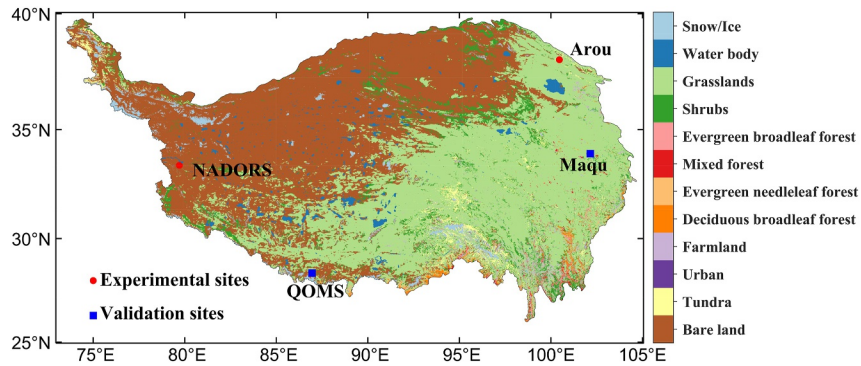

Figure 1. Spatial distribution of the land cover types and field sites over the Tibetan Plateau.

selects bare land and alpine grassland underlying surfaces as research objects, and the main research period is from May to September with relatively little snow cover.

3. Data, Model, Albedo Schemes, Numerical Experimental Design, and Methods

3.1. Data

The data sets used in this study are listed as follows:

1. The observation data from four field stations, including Arou (38.05°N, 100.46°E) and Maqu (33.92°N, 102.15°E) stations featured by alpine grassland, NADORS (33.39°N, 79.70°E) and QOMS stations (28.36°N, 86.95°E) featured by bare land (Figure 1). The available observed data include atmospheric data (2 m air temperature and air relative humidity, precipitation, surface air pressure, 2 m wind speed, surface upward and downward shortwave radiation and downward longwave radiation) and flux data (sensible and latent heat fluxes). The data from the Arou (Maqu) station with a temporal resolution of half-hour during 1 January 2013–31 December 2014 (1 January 2014–31 December 2015), and data from the NADORS (QOMS) station with a temporal resolution of 1 hr during 1 January 2012–31 December 2013 (1 January 2008–31 December 2009). The half-hourly (hourly) soil temperature and moisture data observed at Arou (NADORS) station at the depths of 0, 0.02, 0.1, 0.2, 0.4, 0.6, 1.2, 1.6, and 2 m (0, 0.2, 0.5, 1, and 2 m) during 1 January 2013–31 December 2014 (1 January 2012–31 December 2013). All the albedo data are calculated based on the upward and downward shortwave radiation observation data at each station. All observational data were quality controlled for spatiotemporal consistency and logical extreme values, with unqualified data corrected or eliminated. Missing data were filled by interpolating from adjacent observational records. It is worth noting that the observation data from Arou and NADORS stations are used for the establishment of the new albedo schemes and model evaluation, but the observation data from Maqu and QOMS stations are only used to validate the simulation results of the new albedo schemes.
2. The 3-hourly China Meteorological Forcing Data set (CMFD) (Yang et al., 2019) with a horizontal spatial resolution of 0.1° includes 7 variables: 2 m air temperature and specific humidity, surface air pressure, 10 m wind speed, surface downward solar and longwave radiation, and precipitation rate. This study used the CMFD data from 1 January 1997 to 31 December 2016 to drive the CLM5 model in the regional simulations.
3. The surface temperature data is obtained from the China Meteorological Administration Land Data Assimilation System (CLDAS) surface temperature analysis product data set provided by the China Meteorological Data Service Centre. The data set covers the Asian region with a temporal resolution of 1 hr and a horizontal resolution of 0.0625° (Sun et al., 2017). This study used the CLDAS data between 1 January 2010 and 31 December 2015 for analysis, and the bilinear interpolation method was employed to resample the data to a spatial resolution of 0.1° to facilitate comparison with the simulated data.

3.2. Model Description

The Community Land Model (CLM) is a component of the land surface processes in the Community Earth System Model. It combines the advantages of many previous land surface models, comprehensively considers multiple processes such as the physics, hydrology, biochemistry, and material cycling of the land surface, and

incorporates many new sub-models. It is currently the most well-developed and widely used land surface model in the world (Lawrence et al., 2019; Luo et al., 2023; Xie et al., 2019). The CLM5 used in this study is the latest version (https://www.cesm.ucar.edu/models/cesm2/land). This version mainly improves the main dynamic processes such as soil and vegetation hydrological processes and snow melting dynamic processes. It is more suitable for the research of land surface processes related to permafrost, forest fires, urban canopies, etc. In the CLM5, the grid-scale surface albedo is obtained by weighted summation based on different types of land cover (bare land, vegetation and snow surface) within each model grid. The default 20 soil layers are set at the depths of 0.01, 0.04, 0.09, 0.16, 0.26, 0.40, 0.58, 0.80, 1.06, 1.36, 1.70, 2.08, 2.50, 2.99, 3.58, 4.27, 5.06, 5.95, 6.94, and 8.03 m (Bao et al., 2024).

3.3. Albedo Parameterization Schemes

3.3.1. Albedo Parameterization Schemes in the CLM5

In the CLM5 model, incident solar radiation is divided into direct and diffuse radiation (f), each further divided into visible radiation (VIS, <0.7 μm) and near-infrared radiation (NIR, >0.7 μm) according to the wavelength (Λ). The albedos of direct visible radiation (α_{vis}), direct near-infrared radiation (α_{nir}), diffuse visible radiation ($\alpha^{\mu}_{\text{vis}}$), and diffuse near-infrared radiation ($\alpha^{\mu}_{\text{nir}}$) are calculated separately.

$$SR = NIR + NIR^{f} + VIS + VIS^{f} \tag{1}$$

$$FSR = \alpha SR = \alpha_{\text{nir}} NIR + \alpha_{\text{vis}} VIS + \alpha^{f}_{\text{nir}} NIR^{f} + \alpha^{f}_{\text{vis}} VIS^{f} \tag{2}$$

where SR and FSR are incident solar radiation and reflected solar radiation, respectively. α is the albedo of total incident solar radiation.

The albedo of bare land is specified as a function of soil color and soil moisture:

$$\alpha_{c} = 0.11 - 0.4 \times \text{ssw} \tag{3}$$

$$\alpha^{f}_{\text{soi},\Lambda} = \alpha_{\text{soi},\Lambda} = \min(\alpha_{\text{sat},\Lambda} + \alpha_{c}, \alpha_{\text{dry},\Lambda}) \tag{4}$$

where ssw is the soil moisture content in the top layer, and α_{c} represents the decrease in soil albedo caused by soil moisture. $\alpha^{f}_{\text{soi},\Lambda}$ and $\alpha_{\text{soi},\Lambda}$ are the albedos of diffuse and direct solar radiation with different wavelengths on the soil surface, respectively. $\alpha_{\text{sat},\Lambda}$ and $\alpha_{\text{dry},\Lambda}$ are the albedo of the soil in saturated and dry states respectively and are directly given as a constant based on soil colors (the soil color is divided into 20 color types in CLM5).

For the vegetation underlying the surface, the two-stream approximation method for calculating the atmospheric radiation transmission is introduced into the calculation of vegetation canopy radiation transmission (Dickinson et al., 1983; Oleson et al., 2008, 2010). As shown in the following basic equations of radiation transfer (Equations 5 and 6), the model divides the transmission process into three parts: extinction, primary scattering and multiple scattering:

$$-\overline{\mu}\frac{dI\uparrow}{d(L+S)} + [1-(1-\beta)\omega]\, I\uparrow - \omega\beta I\downarrow = \omega\overline{\mu}K\beta_{0}e^{-K(L+S)} \tag{5}$$

$$\overline{\mu}\frac{dI\downarrow}{d(L+S)} + [1-(1-\beta)\omega]\, I\downarrow - \omega\beta I\uparrow = \omega\overline{\mu}K\left(1-\beta_{0}\right)e^{-K(L+S)} \tag{6}$$

where $I\uparrow$ and $I\downarrow$ refer to the upward and downward diffuse solar radiative flux per unit incident radiant flux, respectively. $K = \mathrm{G}(\mu)/\mu$, $G(\mu)$, $\overline{\mu}$, ω, β, β_{0} and are the vegetation optical parameters calculated based on the work of Sellers (1985), μ is the sine of the solar elevation angle, L and S indicate the leaf and stem area index, respectively. By assuming the upward and downward diffusion fluxes are completely isotropic, the canopy radiative transfer equations are solved by parametrizing the individual single scattering albedo ($a_{s}(\mu)_{\Lambda}$) of leaves at the upper and lower boundary conditions of the vegetation canopy. The upscatter for diffuse radiation and direct radiation are given as follows:

$$\omega_{\Lambda}^{\mathrm{veg}}\beta_{\Lambda}^{\mathrm{veg}} = \frac{1}{2}\left[\alpha_{\Lambda} + \tau_{\Lambda} + (\alpha_{\Lambda} - \tau_{\Lambda})\cos^2\overline{\theta}\right] \tag{7}$$

$$\omega_{\Lambda}^{\mathrm{veg}}\beta_{0,\Lambda}^{\mathrm{veg}} = \frac{1 + \overline{\mu}K}{\overline{\mu}K}a_s(\mu)_{\Lambda} \tag{8}$$

where α_{Λ} is a weighted combination of the leaf and stem reflectance ($\alpha_{\Lambda}^{\mathrm{leaf}}$, $\alpha_{\Lambda}^{\mathrm{stem}}$) and τ_{Λ} is a weighted combination of the leaf and stem transmittance ($\tau_{\Lambda}^{\mathrm{leaf}}, \tau_{\Lambda}^{\mathrm{stem}}$), $\overline{\theta}$ is the mean leaf inclination angle relative to the horizontal plane:

$$\alpha_{\Lambda} = \alpha_{\Lambda}^{\mathrm{leaf}}\omega_{\mathrm{leaf}} + \alpha_{\Lambda}^{\mathrm{stem}}\omega_{\mathrm{stem}} \tag{9}$$

$$\tau_{\Lambda} = \tau_{\Lambda}^{\mathrm{leaf}}\omega_{\mathrm{leaf}} + \tau_{\Lambda}^{\mathrm{stem}}\omega_{\mathrm{stem}} \tag{10}$$

$$\omega_{\mathrm{leaf}} = L/(L+S) \tag{11}$$

$$\omega_{\mathrm{stem}} = S/(L+S) \tag{12}$$

$$\cos\overline{\theta} = \frac{1 + \chi_L}{2} \tag{13}$$

The model divides vegetation into different plant functional types (PFTs), and the optical parameters (χ_L, $\alpha_{\Lambda}^{\mathrm{leaf}}$, $\alpha_{\Lambda}^{\mathrm{stem}}$, $\tau_{\Lambda}^{\mathrm{leaf}}$, $\tau_{\Lambda}^{\mathrm{stem}}$) of different PFTs are given as constants. Through complex derivation, the upward and downward radiation fluxes of vegetation with only scattered radiation and only direct radiation can be obtained (Zhou et al., 2008). More information about the canopy radiative transfer can refer to the CLM5 technical note, which is available at the website https://escomp.github.io/ctsm-docs/versions/release-clm5.0/html.

3.3.2. Newly Developed Albedo Parameterization Schemes

Previous studies have shown that soil moisture and solar elevation angle are two important factors affecting the albedo. For the underlying surface of vegetation with a high canopy, the near canopy surface air relative humidity is also an important factor affecting the canopy surface albedo (Wang et al., 2024). However, the influence of soil liquid content on the surface albedo is weakened due to the existence of frozen soil on the TP. So, can the change of soil ice content affect the albedo? Therefore, this study conducts partial correlation of albedo with the sine of solar elevation angle, the 2m air temperature and wind speed, air relative humidity, the soil liquid content at 0 cm depth (when soil temperature is greater than 0°C) and soil ice content at 0 cm (2 cm) depth (when soil temperature is less than 0°C) based on the observation data at Arou (NADORS) sites. It was found that through partial correlation analysis, the solar elevation angle, soil ice content, and near canopy surface air relative humidity (soil liquid content) were the main factors affecting the albedo of the grassland (bare land) in the TP. From the relationship between albedo and these factors (Figure 2), it can be seen that the albedo decreases exponentially with the increase of sine of solar elevation angle (Figures 2a and 2b), increases linearly with the increase of soil ice content (Figures 2c and 2d), and decreases linearly with the increase of near surface air relative humidity and soil liquid content (Figures 2e and 2f). Therefore, we proposed two new albedo schemes for the bare land underlying surface and alpine grassland underlying surface, which are called BN scheme and GN scheme for simplicity.

Due to the paucity of observation data for visible radiation and near-infrared radiation at field stations, the direct and diffuse radiation are even more rare; therefore, it is not feasible to study the albedo of these four parts of solar radiation separately. As shown in Equation 2, it is feasible to multiply a correction factor on both the left (α) and the right side of equation ($\alpha_{\mathrm{nir}}, \alpha_{\mathrm{vis}}, \alpha_{\mathrm{nir}}^{f}, \alpha_{\mathrm{vis}}^{f}$) to make the albedo obtained by the model closer to the observation. For the albedo scheme of grassland, referring to the method proposed by Wang et al. (2024), it is planned to introduce the influence of the midday solar elevation angle of each day, near surface air relative humidity and soil ice content by multiplying some correction factors with the simulated albedo by the original albedo scheme (Equation 14). For the albedo scheme of the bare land, referring to the method proposed by Zheng et al. (2017) and Equations 3 and 4, the impacts of solar elevation angle, soil liquid content and soil ice content on albedo are introduced based on the albedo when the soil is saturated (Equation 15). The following empirical relationship equations were obtained by fitting:

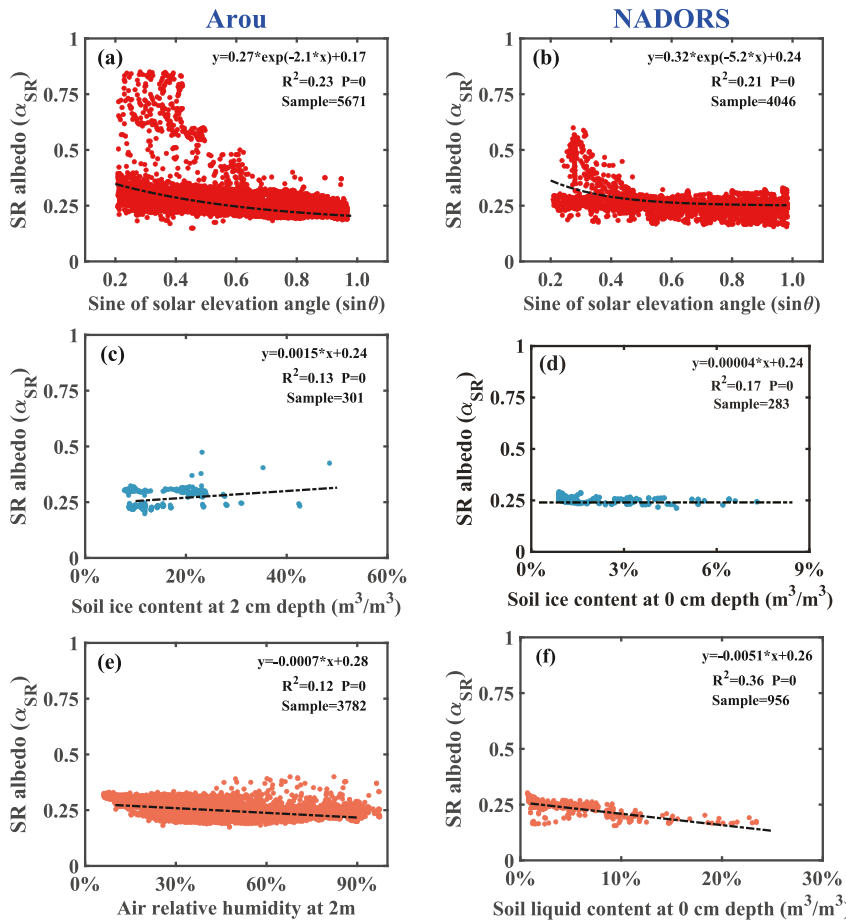

Figure 2. The relationship of (a) the sine of solar elevation angle, (c) soil ice content at 2 cm depth and (e) 2 m air relative humidity ((b) the sine of solar elevation angle, (d) soil ice content and (f) soil liquid content at 0 cm depth) with the surface albedo under snow free conditions based on the half-hourly (hourly) observations during the months between May and September of 2013–2014 (2012–2013) at Arou station featured by grassland (NADORS station featured by bare land).

$$\alpha_{\text{grass},\Lambda} = \alpha_{y,\Lambda} \times \exp(-0.89 \times \sin\theta_m) \times (1 + 0.34 \times \text{ice}) \times (1 - 0.002 \times rh) \times 3.22 \quad (14)$$

$$\alpha_{\text{bare},\Lambda} = \min\left(\alpha_{\text{sat},\Lambda} + 0.135 \times \exp(-0.55 \times \sin\theta) + 0.34 \times \text{ice} - 0.002 \times \text{liq}, \alpha_{\text{dry},\Lambda}\right) \quad (15)$$

Where $\alpha_{y,\Lambda}$ represents the albedo of shortwave radiation simulated by the original albedo scheme of grassland (Equations 7 and 8) in the CLM5 model, $\alpha_{sat,\Lambda}$ represents the albedo of the soil in saturated states. θ (radian) is the solar elevation angle, θ_m (radian) is the midday solar elevation angle at each day of a year, and rh (%) is the air relative humidity near the canopy surface, *ice* and *liq* (kg/m^2) are the content of ice and liquid water in the top soil layer simulated by CLM5. The correlation coefficients of the albedos calculated by Equations 14 and 15 with the observations are 0.54 and 0.64, both of which are above the significance level of 95%.

3.4. Numerical Experimental Design

To verify the improvement level of the GN and BN schemes in simulating the albedo of alpine grassland and bare land on the TP under snow free conditions relative to the original albedo schemes in the CLM5 model, we conducted control and sensitivity single-point experiments at Arou station featured by alpine grassland and the NADORS station featuring bare land, respectively. In addition, due to the GN and BN schemes constructed based on the observation data at Arou and NADORS stations, respectively, to better evaluate the applicability of the newly developed albedo schemes at other stations, we also conducted control and sensitivity single-point

experiments at Maqu (alpine grassland) and QOMS (bare land) stations, respectively. Details of the model configuration for each experiment are shown as follows:

For simplicity, the single-point control (sensitivity) experiments for grassland and bare land are called CEG and CEB (SEG and SEB), respectively. The CEG (CEB) experiments at Arou and Maqu (NADORS and QOMS) stations were carried out by the CLM5 model adopting the original grassland (bare land) albedo scheme, while the SEG (SEB) experiments at Arou and Maqu (NADORS and QOMS) stations were conducted by the CLM5 model using the GN (BN) albedo scheme constructed in this study.

For all the single-point experiments mentioned above, the CLM5 model ran 12 years cyclically driven by the 2-year field observed atmospheric forcing data observed at each station (details can be found in Section 3.1) and output hourly results, and the model results of the last 2 years are extracted for subsequent analysis.

In addition, to evaluate the suitability of the newly developed albedo schemes across the TP region, this study also conducted a set of regional experiments with the model domain covering the entire TP, namely CTRL and SEXP experiments. In the CTRL (SEXP) experiment, driven by the 3-hourly CMFD atmospheric forcing data during 1 January 1997–31 December 2016 (details can be found in Section 3.1), simulations of 20 years were carried out by the CLM5 model adopting the original (newly developed) albedo schemes for grassland and bare land and output daily results, and the simulations of the last 10 years were extracted for further analysis.

3.5. Analysis Methodology

In this study, we used the root mean square error (RMSE) between the simulations and the observations to evaluate the model performance in detecting the quantity, and the Taylor score (TS; Taylor, 2001) to evaluate the model ability to simulate both the amplitude and pattern of variability simultaneously.

The calculation of RMSE is given by

$$RMSE = \left[\frac{1}{N}\sum_{i=1}^{N}(S_i - O_i)^2\right]^{1/2} \tag{16}$$

Where S_i and O_i are the simulations and observations, respectively, and N is sample size. The RMSE approaching nearer to 0 indicates a smaller difference between simulations and observations and consequently higher simulation accuracy.

The calculation of TS is given by

$$TS = \frac{4*(1+r)}{\left(SDR + \frac{1}{SDR}\right)^2(1+r_0)} \tag{17}$$

$$r = \frac{\frac{1}{N}\sum_{i=1}^{N}(S_i - \overline{S})*(O_i - \overline{O})}{\left[\frac{1}{N}\sum_{i=1}^{N}(S_i - \overline{S})^2\right]^{1/2}\left[\frac{1}{N}\sum_{i=1}^{N}(O_i - \overline{O})^2\right]^{1/2}} \tag{18}$$

$$SDR = \frac{\left[\frac{1}{N}\sum_{i=1}^{N}(S_i - \overline{S})^2\right]^{1/2}}{\left[\frac{1}{N}\sum_{i=1}^{N}(O_i - \overline{O})^2\right]^{1/2}} \tag{19}$$

Where r represents the correlation between simulations and observations, and r_0 is the theoretical maximum correlation and it is set to 1 here. The SDR represents the ratio of standard deviation of simulations to the standard deviation of observations, $\overline{S}$ ($\overline{O}$) represents the average of simulations (observations) with sample size of N. TS ranges from 0 to 1, and larger TS indicates better performance.

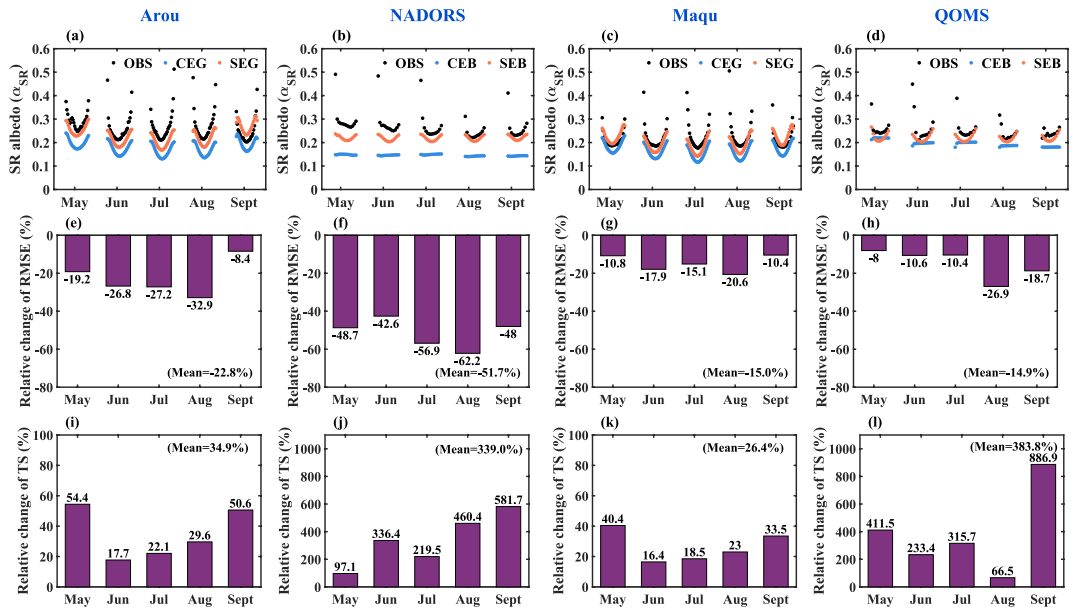

Figure 3. The diurnal variation of simulated and observed surface albedo in each month at each station from May to September for 2 years (a–d). The relative changes of RMSE and TS of the simulated surface albedo in the sensitivity experiments compared to those in the control experiments in each month (e–l). The relative changes of RMSE (TS) averaged over May to September are listed at the bottom (top) right-hand corner of each sub-figure of (e–l).

4. Results

4.1. Albedo, Surface Thermal Conditions and Soil Temperature Simulations of the Two Typical Land Surfaces Improved by the Newly Developed Albedo Schemes

From Figures 3a–3d, the observed albedos at the four stations consistently present a "U" -shaped variation with high values in the morning and evening and low values at noon. Compared to the observations, the CEG experiment can reproduce this diurnal variation pattern of the albedo in grassland, but the CEB experiment cannot reproduce this diurnal variation pattern of albedo in bare land. This may be related to the fact that the influence of solar elevation angle on albedo is considered in the original albedo scheme of grassland but not in the original albedo scheme of bare land. Compared to the CEG and CEB experiments, the SEG and SEB experiments adopting the newly developed albedo schemes not only produce the albedo much closer to the observations but also better simulate the pattern of albedo diurnal variation, especially at the bare land.

From Figures 3e–3l, the RMSE (TS) produced by the new albedo schemes are significantly reduced (increased) compared to the original albedo schemes. The reduction of RMSE (increase of TS) ranges from ∼10% to ∼60% (∼20%–∼900%) during May to September across the four stations. Much higher improvements of TS induced by the new albedo scheme of bare land can be noted at the NADORS and QOMS stations, with the mean relative change of TS during May to September being more than 300% (Figures 3j and 3l). Moreover, although the GN and BN albedo schemes were developed based on the observations at Arou and NADORS stations, applications of them can lead to the RMSE (TS) of surface albedo simulation at Maqu and QOMS stations decreased (increased) by an average of ∼15% (∼26%) from May to September, suggesting that the newly developed albedo schemes show good suitability on the TP to some extent.

The improvement in the simulations of albedo may further affect the simulations of surface thermal conditions by affecting the surface radiation energy balance. As shown in Equation 20, the net shortwave radiation (NSR) and net longwave radiation (NLR) received at the surface are released through sensible heat flux (SH), latent heat flux (LH) and ground heat flux (GH):

$$NSR - NLR = NR = SH + LH + GH \quad (20)$$

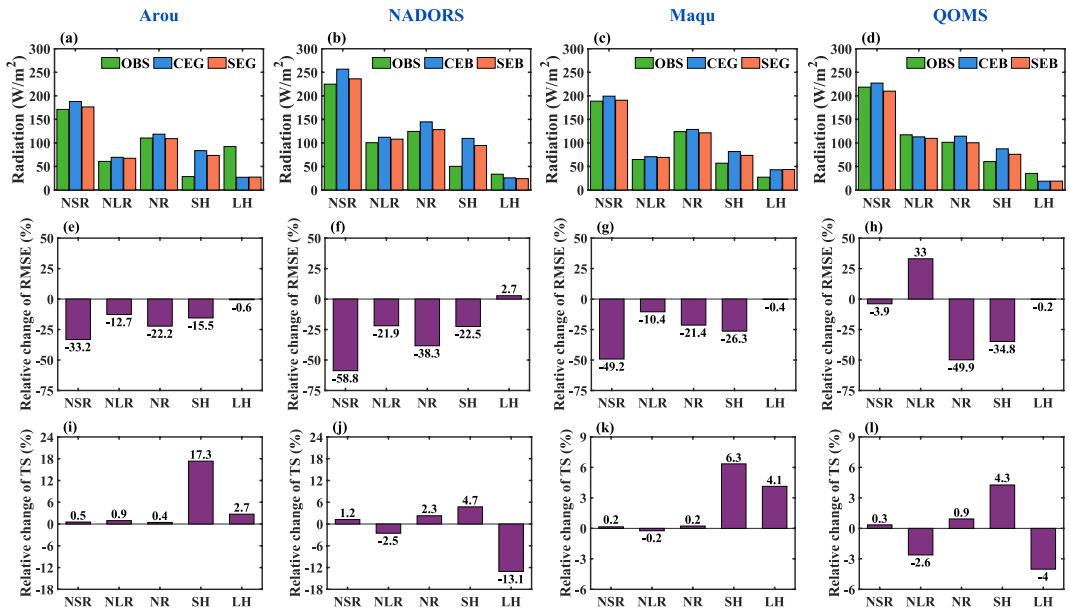

Figure 4. Each component of the surface heat balance averaged over May to September for 2 years at each station from the observations and the simulations of different experiments (a–d). The relative changes of RMSE and TS of the surface radiation and heat flux simulations in the sensitivity experiments relative to those produced by the control experiments (e–l).

Where the net radiation (NR), NSR, GH are positive downward and NLR, SH and LH are positive upward at the surface.

As shown in Figures 4a–4d, the original albedo schemes of the CLM5 model clearly tend to overestimate the NSR and NR at bare land and grassland surfaces; this is mainly due to the underestimated albedo (Figure 3). The overestimation of NSR (NR) can be clearly reduced by the new albedo schemes, further leading to the decrease of surface temperature and thereafter reduced NLR. Overall, the improvements of the NR simulations induced by the new albedo schemes are mainly result from the improved NSR simulations, whose RMSE can be reduced by ∼20%–∼50% at the four stations relative to the original albedo schemes, but with very slight improvements of TS (less than 2%).

In addition, the CLM5 with the original albedo schemes tends to overestimate (underestimate) the surface sensible (latent) heat flux (Figures 4a–4d). Adopting the new albedo schemes can clearly improve the simulation of surface sensible heat flux with the RMSE reduction (TS increase) ranging from ∼20% to ∼30% (∼5%–∼15%) across the four stations compared to the original albedo schemes (Figures 4e–4l). However, the improvements in the surface latent heat flux induced by the new albedo schemes are marginal.

As a whole, adopting the new albedo schemes can lead to improved simulations of NR and surface thermal conditions, thereby mainly resulting in the improvements of the land-air sensible heat transfer.

Corresponding to the changes in surface NR, the land surface temperature (LST) and soil temperature at different depths (Figures 5 and 6) change accordingly. As shown in Figures 5a and 5b, the observed LST at both sites gradually increases from May to July and decreases from August to September; the CLM5 model adopting the original albedo schemes for the bare land and grassland surfaces can well reproduce this trend but it clearly overestimates the LST, especially in August and September. Relative to the original albedo schemes, adopting the new albedo schemes can reduce the overestimation of LST to some extent (Figures 5c and 5d), and the RMSE of the LST simulations can be reduced by ∼6%–∼30% in different months at the stations with relatively larger reduction at the NADORS station but with very slight improvements of TS (less than 1.5%) (Figures 5e–5h). Overall, improvements in reproducing the LST in quantity induced by the adoption of new albedo schemes are much more obvious than reproducing the amplitude and pattern of variability of LST.

Taking the soil temperature observation depths at the stations as the reference, we selected the simulated soil temperature data at depths closest to the observational depths, derived the corresponding values through

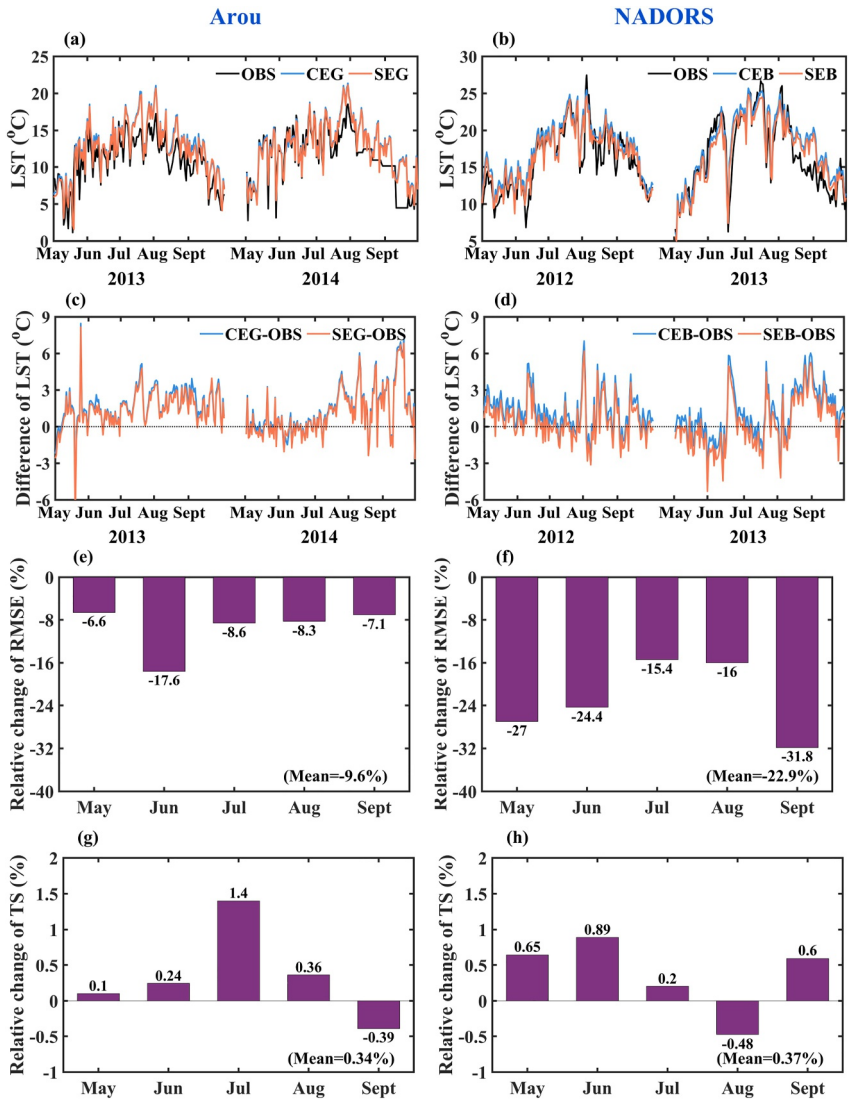

Figure 5. The time series of the LST from observations and simulations of control experiments and sensitivity experiments and the differences between simulations and observations at Arou and NADORS over May to September of 2 years (a–d). The relative changes of RMSE and TS of the LST simulated by the sensitivity experiments relative to those produced by the control experiments (e–h), and the relative changes of RMSE and TS averaged over May to September are listed at the bottom right-hand corner of each sub-figure of (e–h).

interpolation, and then compared them with the observed soil temperatures. From Figures 6a and 6b, the soil temperature decreases with the depth and is characterized by a warmer upper layer of 0–100 cm and a cooler lower layer below 100 cm. In addition, similar to the surface temperature, the soil temperature also shows a trend of increasing first and then decreasing from May to September, but there is a significant lag. As soil depth increases, the lag of this change becomes more apparent. The CLM5 with the original albedo schemes tends to overestimate the soil temperature (especially below the depth of 20 cm in May) at different depths (Figures 6e and 6f) due to the overestimation of the NR (Figures 4a and 4b). By adopting the new albedo schemes, the CLM5 can improve the time-depth distribution of soil temperature simulations and reduce the warm biases produced by adopting the original albedo schemes by ∼0.2°C–∼1°C with relatively larger improvements at the bare land (Figures 6g and 6h).

As shown in Figures 7a and 7d, the CLM5 with the new albedo schemes can reduce the RMSE of soil temperature profile simulations ranging from 0.1°C to 0.3°C (0.3°C–0.6°C) at Arou (NADORS) station, and the RMSE can be reduced by more than 10% at all depths (Figures 7c and 7f). From Figures 7b and 7e, the TS of soil temperature

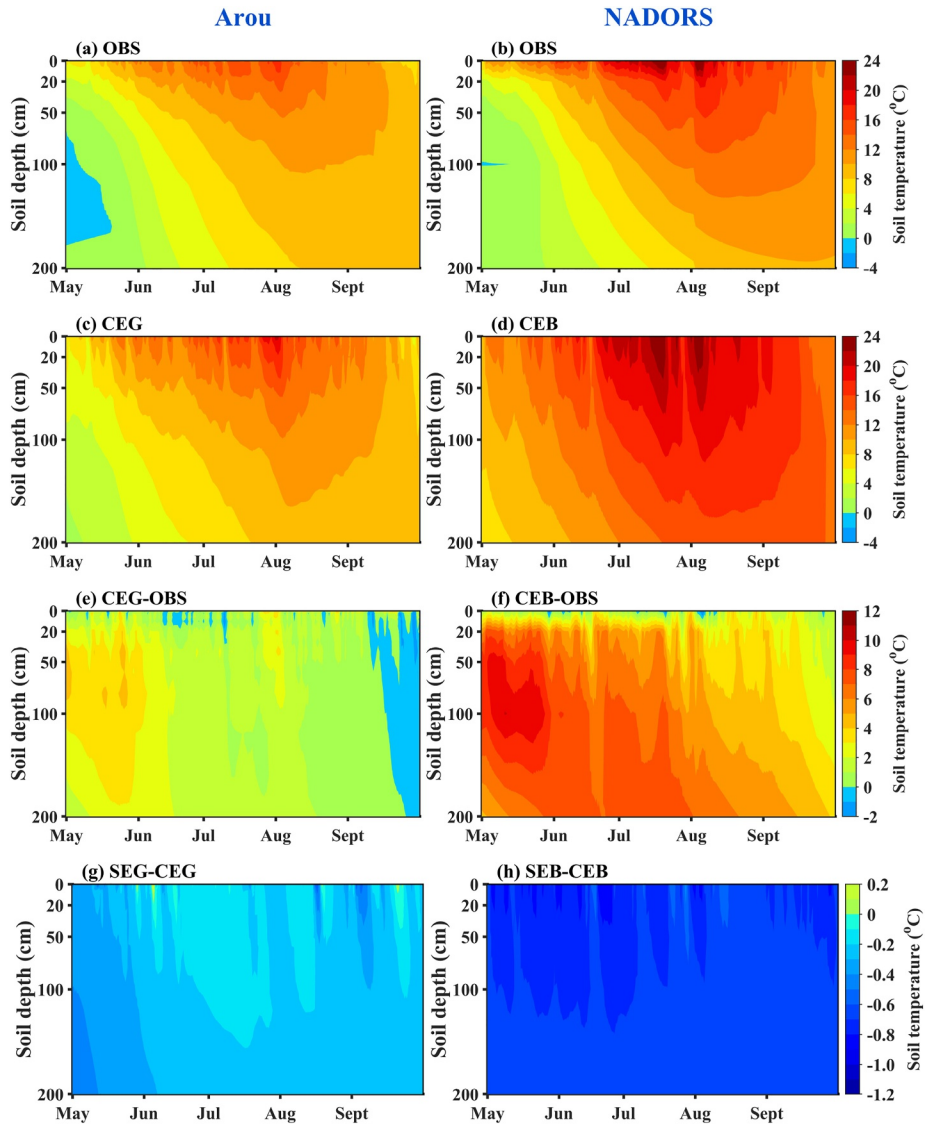

Figure 6. The temporal variation of the observed and simulated soil temperature profiles at Arou and NADORS stations over May to September (a–d). The temporal variation of soil temperature differences between control experiment simulations and the observation (e and f), and between the sensitivity and control experiments (g and h) over May to September.

simulations at all depths is generally higher than 0.8, indicating that the CLM5 can simulate the amplitude and pattern of the soil temperature variation well. Relative to the original albedo scheme, the new albedo schemes tend to produce slightly higher TS of soil temperature simulations, but the relative changes of TS are less than 2% (Figures 7c and 7f). Overall, the new albedo schemes show better performance to improve the soil temperature simulations in quantity than in the temporal variation.

4.2. Impact of the New Albedo Schemes on the Surface Thermal Condition Simulations in the TP During Snow Free Seasons

To evaluate the impact of the new albedo schemes on the simulation of surface thermal conditions on the TP, we conducted a set of regional comparative simulation experiments (CTRL and SEXP). As shown in Figures 8a, 8c and 8d, it can be seen that the differences in NSR and NR, SH between the SEXP experiment and CTRL experiment show similar spatial patterns. Relatively larger differences are located in the northwest and southwest TP, and relatively lower differences are concentrated in the southeast TP, which is consistent with the results of Figure 4. The difference in NLR (Figure 8b) is much lower than those of NSR, and the difference in LH and GH

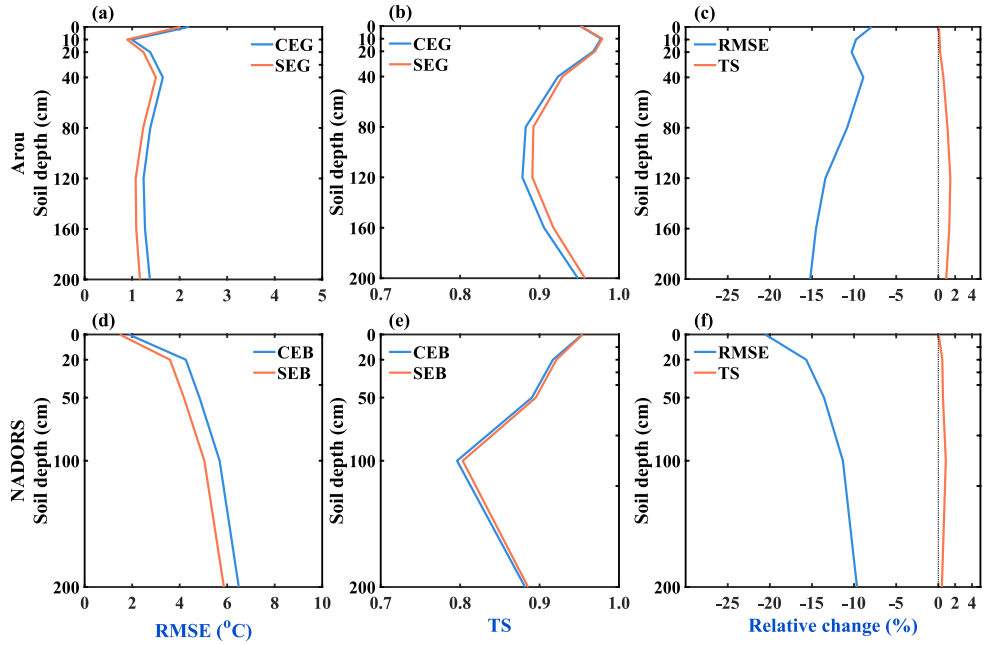

Figure 7. The RMSE (a and d) and TS (b and e) for the simulated soil temperature at different depths over May to September of the 2 years from control experiment and sensitivity experiment and their changes produced by the sensitivity experiments relative to the control experiments (c and f).

(Figures 8e and 8f) is much less than those in SH, indicating that the changes in NR mainly come from the change in NSR and predominantly affect the changes of surface sensible heat flux.

To further quantify the influence of the new albedo schemes on the simulations of surface thermal conditions, the TP regional mean differences in the NSR, NLR, NR, SH, LH and the total of SH, LH and GH between the SEXP experiment and CTRL experiment and their relative changes were further calculated. As shown in Figure 9a, relative to the CTRL experiment adopting the original albedo schemes, adopting the new albedo schemes in the SEXP experiment can lead to the simulated NSR, NLR and NR decreased by 9.09, 2.48, and 6.61 W/m^2, respectively, and the change of the NR (reduction of 6.61 W/m^2) is mainly balanced by the change of SH (6.06 W/m^2), which shows the largest relative change of ∼15% among the five surface heat components (Figure 9b).

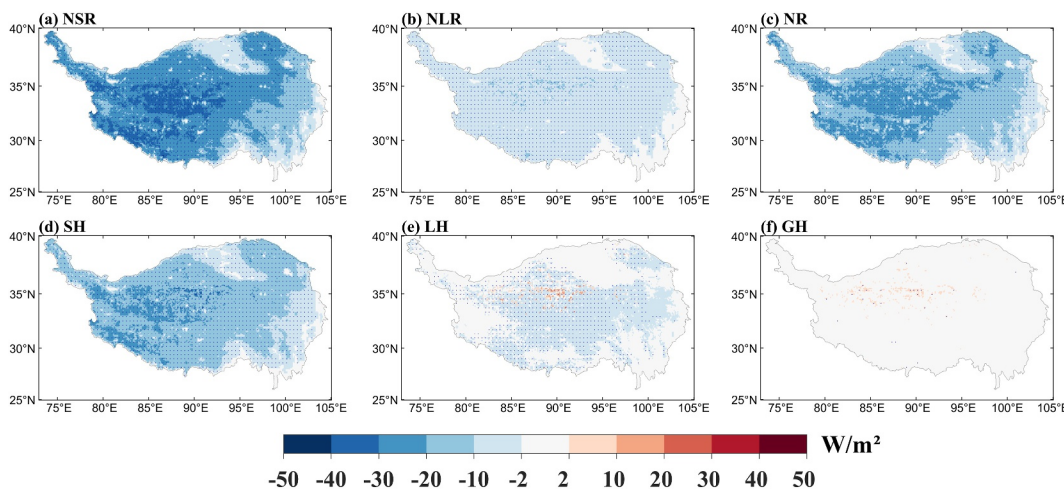

Figure 8. The differences in each component of surface heat balance between the SEXP experiment and CTRL experiment averaged over May to September of 2007–2016. The black dots in panels indicate the confidence level above 95% of t test.

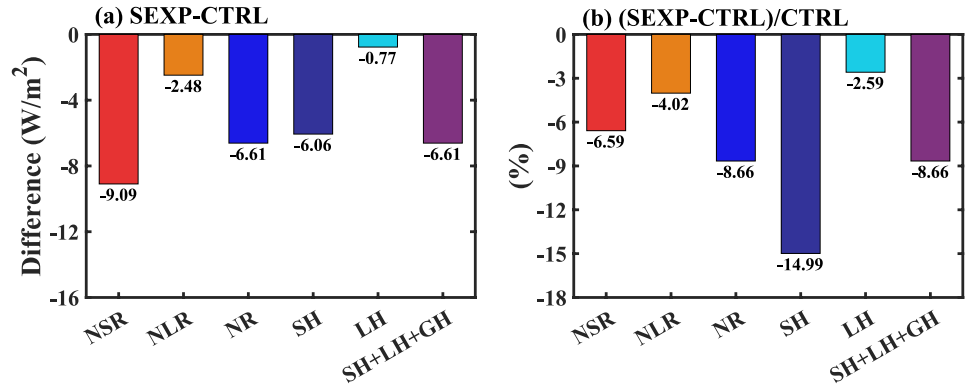

Figure 9. The mean differences of each surface heat component during May to September of 2007–2016 between the SEXP and CTRL experiments regionally averaged over the TP and the relative changes produced by the SEXP experiment compared to the CTRL experiment.

From Figures 10a and 10b, the CTRL experiment can overall simulate the spatial distribution of LST over the TP, but overestimates the LST in most regions of the central and western TP (Figure 10c) due to the overestimation of NR (Figure 8c). This LST overestimation can be clearly reduced by adopting the new albedo schemes (Figure 10d). Correspondingly, the surface sensible heat flux decreased with the LST reduced in the SEXP experiment (Figure 8d). From Figures 10e–10h, compared to adopting the original albedo schemes, adopting the new albedo schemes can clearly reduce (slightly increase) the RMSE (TS) of mean LST simulations during May to September on the TP by ∼4%–∼15% (less than 1%); this is similar to the situations of single-point simulations, adopting the new albedo schemes tends to improve the LST simulations in quantity than in the spatial pattern.

5. Conclusions

This study used field observation data to identify the main factors affecting the albedos of the bare land and alpine grassland, which are widely distributed on the TP, and constructed two new albedo schemes suitable for the bare land and grassland on the TP under snow free conditions, respectively. The main findings are listed as follows:

The CLM5 model with the original albedo schemes for the bare land and alpine grassland clearly underestimates the albedo over the TP, and cannot reproduce the diurnal variation of bare land surface albedo. In-depth analysis of the relationship of observed albedo with potential impact factors indicates that the solar elevation angle, soil ice content, and air relative humidity (the solar elevation angle, soil ice content, and soil liquid content) are the main factors affecting the albedo of the grassland (bare land) on the TP. Two new albedo schemes have been constructed for the bare land and grassland, respectively.

By introducing the newly developed albedo schemes into the CLM5 model for single-point simulation evaluation at four stations, the evaluation results show that adopting the new albedo schemes can clearly improve the simulation accuracy of the albedo on the bare land and alpine grassland, especially that the diurnal variation of albedo of the bare land can be well reproduced. The RMSE (TS) produced by the new albedo schemes are significantly reduced (increased) by ∼10%–∼60% (∼20%–∼900%) among the four field stations compared to the original albedo schemes.

The improvement of the albedo simulation further reduces the overestimation of NR by the original albedo schemes, thereby mainly resulting in the improvements of the land-air sensible heat transfer. By adopting the new albedo schemes, the RMSE of simulated NR (SH) can be reduced by ∼20%–∼50% (∼20%–∼30%) at the four stations relative to the original albedo schemes, but the improvements of TS are marginal (less than 2%). Furthermore, the improved accuracy of NR simulation achieved by the new albedo schemes significantly mitigated the overestimation of LST and soil temperature. The RMSE of the LST simulations can be reduced by ∼6%–∼30% and the warm biases of soil temperature simulations at different depths can be reduced by ∼0.2°C–∼1°C, and the improvement in quantity is more significant than in time variation.

Regional simulation results show that adopting the new albedo schemes can improve the simulations of NR by increasing the simulation accuracy of albedo, thereby mainly reducing the overestimation of the surface sensible

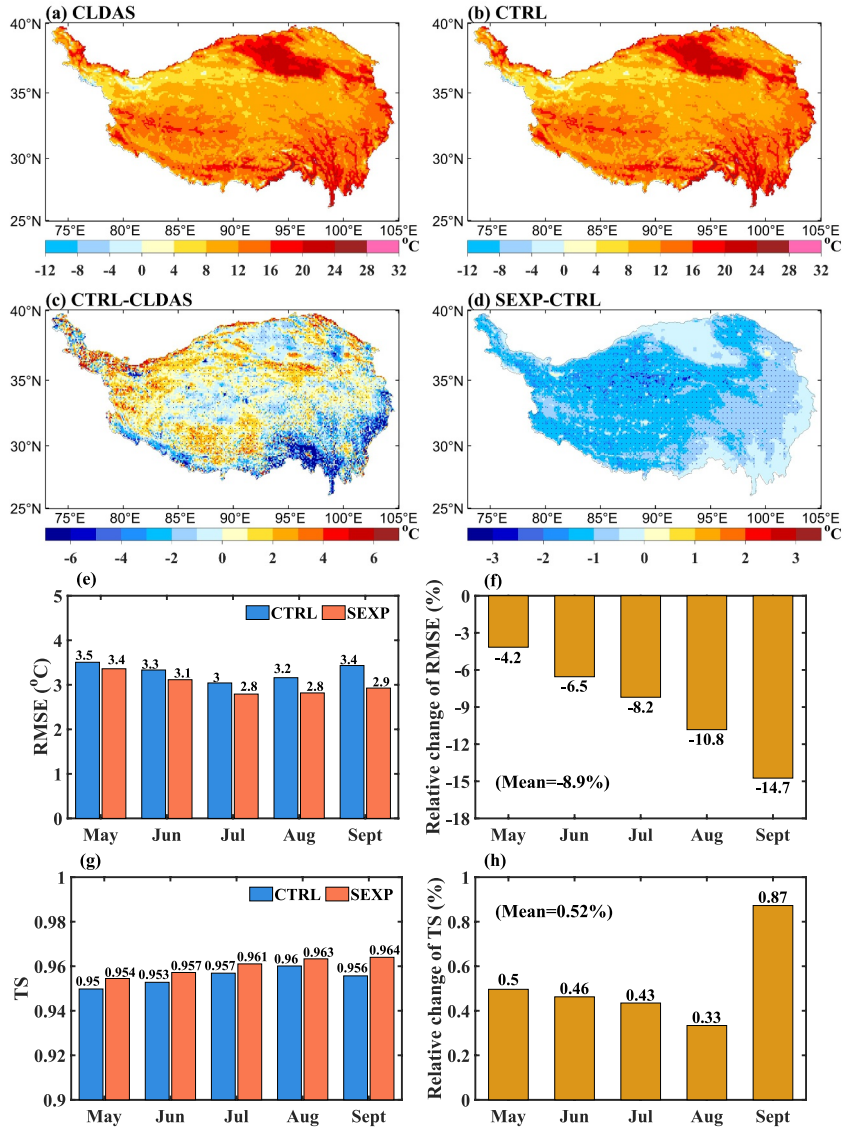

Figure 10. The mean LST during May to September of 2010–2015 from the CLDAS (a) and simulations of the CTRL experiment (b), and the differences between the simulations of the CTRL experiment and the CLDAS (c) and between the SEXP and CTRL experiments (d). The RMSE and TS of the monthly climatic mean LST from May to September over 2010–2015 simulated by the CTRL and SEXP experiments (e) and (g), and their relative changes produced by the SEXP experiment compared to the CTRL experiment (f) and (h). The black dots in panels (c) and (d) indicate the confidence level above 95% of t test. The relative changes of RMSE (TS) averaged over May to September are listed at the bottom (top) left-hand corner of sub-figure of f (h).

heat flux. In addition, adopting the new albedo schemes tends to improve the LST simulations in quantity than in the spatial pattern, with the RMSE (TS) of mean LST simulations during May to September on the TP can be reduced by ∼4%–∼15% (slightly increased less than 1%) compared to the original albedo schemes. Overall, improving the albedo simulation accuracy can significantly enhance the performance of the CLM5 model in simulating surface heat conditions on the TP.

Although the newly developed parameterization scheme can reasonably capture the diurnal variation pattern of albedo, a substantial bias still exists between the simulated and observed values during early morning and late afternoon. This discrepancy is likely attributable to the high proportions of scattered radiation and near-infrared radiation in the incident solar radiation during these two periods. Therefore, it is necessary to further improve the calculation accuracy of the incident radiation partitioning ratio in the model, thereby enhancing the simulation

performance of reflected solar radiation. In addition, the newly developed albedo schemes were only evaluated in the off-line land surface model, and only verified the model's simulation accuracy of surface heat flux and surface thermal conditions on the TP. Future work needs to introduce the new albedo schemes into the regional climate model to explore their impact on the climate simulation in the TP and surrounding regions.

Conflict of Interest

The authors declare no conflicts of interest relevant to this study.

Data Availability Statement

Data-The observation data of the NADORS, QOMS and Maqu stations are from the data set of spatially extensive long-term quality-assured land-atmosphere interactions over the Tibetan Plateau (Ma et al., 2020, 2024; available at https://doi.org/10.5194/essd-12-2937-2020 and https://doi.org/10.5194/essd-16-3017-2024). The data of the Arou station is provided by the Institute of Tibetan Plateau Research, Chinese Academy of Sciences. The driving data used in the regional model simulations is China Meteorological Forcing Dataset (Yang et al., 2019; available at https://doi.org/10.11888/AtmosphericPhysics.tpe.249369.file). The surface temperature data (CLDAS) were provided by the China Meteorological Data Service Centre (available at https://data.cma.cn/). Software—The source codes of Community Land Model version 5 used in this study are freely available online (https://github.com/ESCOMP/CESM).

Acknowledgments
This study is supported by the National Natural Science Foundation of China under Grant 42375157, the Postgraduate Research and Practice Innovation Program of Jiangsu Province, and the Jiangsu Collaborative Innovation Center for Climate Change. We appreciate the High Performance Computing Center of Nanjing University, and the National Key Scientific and Technological Infrastructure project "Earth System Numerical Simulation Facility" (EarthLab) for providing us with computing resources.

References

Bao, Y., Lü, S., Zhang, Y., Meng, X., & Yang, S. (2008). Improvement of surface albedo simulations over arid regions. *Advances in Atmospheric Sciences*, *25*(3), 481–488. https://doi.org/10.1007/s00376-008-0481-y

Bao, Y. Q., Lü, S. h., Liu, Z. S., You, H. Q., & Yang, F. (2024). Numerical simulation of soil temperature and humidity at Maduo station in the source area of the Yellow River by different soil stratification schemes of CLM5.0 land surface model. *Plateau and Mountain Meteorology Research*, *44*(3), 9–16. https://doi.org/10.3969/j.issn.1674-2184.2024.03.002

Cai, F., Zhou, G. S., Ming, H. Q., Li, R. P., Zhang, G., He, Q. J., et al. (2012). A simulative study of effects of dynamic parameterization of surface albedo on land-atmosphere flux exchanges: A case study of rainfed maize field in northeast China. *Acta Meteorologica Sinica*, *70*(5), 1149–1164. https://doi.org/10.11676/qxxb2012.097

Cao, X. Y., Chen, A. J., Xiao, J. S., Bian, L. G., & Zheng, Z. J. (2019). Indicative significance of land Surface Albedo over the Tibetan Plateau to the onset of Plateau summer monsoon. *Climatic and Environmental Research (in Chinese)*, *24*(6), 785–794. https://doi.org/10.3878/j.issn.1006-9585.2019.18153

Cen, S. X., Gong, Y. F., & Lai, X. (2014). Impact of heat source over Qinghai-Xizang Plateau and its surrounding areas on rainfall in Sichuan-Chongqing Basin in summer. *Plateau Meteorology*, *33*(5), 1182–1189. https://doi.org/10.7522/j.issn.1000-0534.2013.00122

Dickinson, R. E. (1983). Land surface processes and climate-surface albedos and energy balance. *Advances in Geophysics*, *25*, 305–353. https://doi.org/10.1016/S0065-2687(08)60176-4

Duan, A. M., Wang, M. R., Lei, Y. H., & Cui, Y. (2013). Trends in summer rainfall over China associated with the Tibetan Plateau sensible heat source during 1980–2008. *Journal of Climate*, *26*(1), 261–275. https://doi.org/10.1175/JCLI-D-11-00669.1

Gu, C., Huang, A., Li, X., & Wu, Y. (2024). The cold bias in the surface air temperature simulations over the Tibetan Plateau of RegCM4 reduced by adopting the 3D sub-grid terrain longwave radiative effect scheme. *Journal of Geophysical Research: Atmospheres*, *129*(23), e2024JD042102. https://doi.org/10.1029/2024JD042102

Guan, X., Huang, J., Guo, N., Bi, J., & Wang, G. (2009). Variability of soil moisture and its relationship with surface albedo and soil thermal parameters over the Loess Plateau. *Advances in Atmospheric Sciences*, *26*(4), 692–700. https://doi.org/10.1007/s00376-009-8198-0

Guo, J. P., Liu, H., An, L. C., Wang, P. X., & Gao, M. (2016). Study on variation of snow cover and its orographic impact over Qinghai-Xizang Plateau during 2001–2012. *Plateau Meteorology*, *35*(1), 24–33. https://doi.org/10.7522/j.issn.1000-0534.2014.00140

Irvine, P. J., Ridgwell, A., & Lunt, D. J. (2011). Climatic effects of surface albedo geoengineering. *Journal of Geophysical Research*, *116*(D24). https://doi.org/10.1029/2011JD016281

Jorgensen, S. V., Cherubini, F., & Michelsen, O. (2014). Biogenic CO_2 fluxes, changes in surface albedo and biodiversity impacts from establishment of a miscanthus plantation. *Journal of Environmental Management*, *146*, 346–354. https://doi.org/10.1016/j.jenvman.2014.06.033

Kala, J., Evans, J. P., Pitman, A. J., Schaaf, C. B., Decker, M., Carouge, C., et al. (2014). Implementation of a soil albedo scheme in the cablev1.4b land surface model and evaluation against MODIS estimates over Australia. *Geoentific Model Development*, *7*(5), 1671–1707. https://doi.org/10.5194/gmd-7-2121-2014

Lawrence, D. M., Fisher, R. A., Koven, C. D., Oleson, K. W., Swenson, S. C., Bonan, G., et al. (2019). The community land model version 5: Description of new features, benchmarking, and impact of forcing uncertainty. *Journal of Advances in Modeling Earth Systems*, *11*(12), 4245–4287. https://doi.org/10.1029/2018ms001583

Li, W., Guo, W., Qiu, B., Xue, Y., Hsu, P. C., & Wei, J. (2018). Influence of Tibetan Plateau snow cover on East Asian atmospheric circulation at medium-range time scales. *Nature Communications*, *9*(1), 4243. https://doi.org/10.1038/s41467-018-06762-5

Liang, S., Wang, K., Zhang, X., & Wild, M. (2010). Review on estimation of land surface radiation and energy budgets from ground measurement, remote sensing and model simulations. *IEEE Journal of Selected Topics in Applied Earth Observations and Remote Sensing*, *3*(3), 225–240. https://doi.org/10.1109/JSTARS.2010.2048556

Liang, X. Z., Xu, M., Gao, W., Kunkel, K., Slusser, J., Dai, Y., et al. (2005). Development of land surface albedo parameterization based on Moderate Resolution Imaging Spectroradiometer (MODIS) data. *Journal of Geophysical Research*, *110*(D11). https://doi.org/10.1029/2004JD005579

Liu, H., Wang, B., & Fu, C. (2008). Relationships between surface albedo, soil thermal parameters and soil moisture in the semi-arid area of Tongyu, northeastern China. *Advances in Atmospheric Sciences*, *25*(5), 757–764. https://doi.org/10.1007/s00376-008-0757-2

Liu, L., Ma, Y., Menenti, M., Su, R., Yao, N., & Ma, W. (2021). Improved parameterization of snow albedo in Noah coupled with Weather Research and Forecasting: Applicability to snow estimates for the Tibetan Plateau. *Hydrology and Earth System Sciences*, *25*(9), 4967–4981. https://doi.org/10.5194/hess-25-4967-2021

Liu, L., Menenti, M., Ma, Y., & Ma, W. (2022). Improved parameterization of Snow Albedo in WRF+Noah: Methodology based on a severe Snow event on the Tibetan Plateau. *Advances in Atmospheric Sciences*, *39*(7), 1079–1102. https://doi.org/10.1007/s00376-022-1232-1

Loarie, S. R., Lobell, D. B., Asner, G. P., Mu, Q., & Field, C. B. (2011). Direct impacts on local climate of sugar-cane expansion in Brazil. *Nature Climate Change*, *1*(2), 105–109. https://doi.org/10.1038/nclimate1067

Luo, J., Huang, A., Jiang, X., Xu, M., Miao, X., Gu, C., & Zhu, X. (2025). The cold biases in the soil and surface air temperature simulations of RegCM4.7 model over the Tibetan Plateau in cold seasons reduced by adopting an improved snow cover fraction scheme. *Journal of Geophysical Research: Atmospheres*, *130*(8), e2025JD043507. https://doi.org/10.1029/2025jd043507

Luo, J., Huang, A., Lyu, S., Lin, Z., Gu, C., Li, Z., et al. (2023). Improved performance of CLM5.0 model in frozen soil simulation over Tibetan Plateau by implementing the vegetation emissivity and gravel hydrothermal schemes. *Journal of Geophysical Research: Atmospheres*, *128*(6), e2022JD038021. https://doi.org/10.1029/2022JD038021

Ma, Y., Xie, Z., Chen, Y., Liu, S., Che, T., Xu, Z., et al. (2024). Dataset of spatially extensive long-term quality-assured land–atmosphere interactions over the Tibetan Plateau. *Earth System Science Data*, *16*(6), 3017–3043. https://doi.org/10.5194/essd-16-3017-2024

Ma, Y. M., Hu, Z. Y., Xie, Z. P., Ma, W., Wang, B., Chen, X., et al. (2020). A long-term (2005–2016) dataset of hourly integrated land–atmosphere interaction observations on the Tibetan Plateau. *Earth System Science Data*, *12*(4), 2937–2957. https://doi.org/10.5194/essd-12-2937-2020

Miao, X., Guo, W., Qiu, B., Lu, S., Zhang, Y., Xue, Y., & Sun, S. (2022). Accounting for topographic effects on snow cover fraction and surface albedo simulations over the Tibetan Plateau in winter. *Journal of Advances in Modeling Earth Systems*, *14*(8), e2022MS003035. https://doi.org/10.1029/2022MS003035

Oleson, K. W., Lawrence, D. M., Bonan, G. B., Flanner, M. G., Kluzek, E., Lawrence, P. J., et al. (2010). *Technical description of version 4.0 of the Community Land Model (CLM)*. National Center for Atmospheric Research. https://doi.org/10.5065/D6FB50WZ

Oleson, K. W., Niu, G. Y., Yang, Z. L., Lawrence, D. M., Thornton, P. E., Lawrence, P. J., et al. (2008). Improvements to the Community Land Model and their impact on the hydrological cycle. *Journal of Geophysical Research*. https://doi.org/10.1029/2007JG000563

Roesch, A., Wild, M., & Ohmura, A. (2001). Snow cover fraction in A general circulation model. In *Remote sensing and climate modeling: Synergies and limitations* (pp. 203–232). https://doi.org/10.1007/0-306-48149-9_9

Roxy, M. S., Sumithranand, V. B., & Renuka, G. (2010). Variability of soil moisture and its relationship with surface albedo and soil thermal diffusivity at Astronomical Observatory, Thiruvananthapuram, south Kerala. *Journal of Earth System Science*, *119*(4), 507–517. https://doi.org/10.1007/s12040-010-0038-1

Sedlar, J., Tjernström, M., Mauritsen, T., Shupe, M. D., Brooks, I. M., Persson, P. O. G., et al. (2011). A transitioning Arctic surface energy budget: The impacts of solar zenith angle, surface albedo and cloud radiative forcing. *Climate Dynamics*, *37*(7–8), 1643–1660. https://doi.org/10.1007/s00382-010-0937-5

Sellers, P. J. (1985). Canopy reflectance, photosynthesis and transpiration. *International Journal of Remote Sensing*, *6*(8), 1335–1372. https://doi.org/10.1080/01431168508948283

Sugathan, N., Biju, V., & Renuka, G. (2014). Influence of soil moisture content on surface albedo and soil thermal parameters at a tropical station. *Journal of Earth System Science*, *123*(5), 1115–1128. https://doi.org/10.1007/s12040-014-0452-x

Sun, S., Jin, J., & Xue, Y. (1999). A simple snow-atmosphere-soil transfer model. *Journal of Geophysical Research*, *104*(D16), 19587–19597. https://doi.org/10.1029/1999JD900305

Sun, S., Shi, C. X., Liang, X., Han, S., Jiang, Z. W., & Zhang, T. (2017). Assessment of ground temperature simulation in China by different land surface models based on station observations. *Journal of Applied Meteorological Science*, *28*(6), 737–749. https://doi.org/10.11898/1001-7313.20170609

Swenson, S. C., & Lawrence, D. M. (2012). A new fractional snow-covered area parameterization for the Community Land Model and its effect on the surface energy balance. *Journal of Geophysical Research*, *117*, D21. https://doi.org/10.1029/2012JD018178

Tang, S., Vlug, A., Piao, S., Li, F., Wang, T., Krinner, G., et al. (2023). Regional and tele-connected impacts of the Tibetan Plateau surface darkening. *Nature Communications*, *14*(1), 32. https://doi.org/10.1038/s41467-022-35672-w

Taylor, K. E. (2001). Summarizing multiple aspects of model performance in a single diagram. *Journal of Geophysical Research*, *106*(D7), 7183–7192. https://doi.org/10.1029/2000JD900719

Tian, L., Chen, J. Q., & Shao, C. L. (2018). Interdependent dynamics of LAI-Albedo across the roofing landscapes: Mongolian and Tibetan plateaus. *Remote Sensing*, *10*(7), 1159. https://doi.org/10.3390/rs10071159

Wang, H., Wei, Z., Huang, A., Li, X., Ma, L., & Guo, S. (2024). Validation of two newly developed albedo schemes based on the observations over the region with evergreen broadleaved forest in Southern China. *Journal of Geophysical Research: Atmospheres*, *129*(1), e2023JD038682. https://doi.org/10.1029/2023JD038682

Wang, S., Trishchenko, A. P., & Sun, X. (2007). Simulation of canopy radiation transfer and surface albedo in the EALCO model. *Climate Dynamics*, *29*(6), 615–632. https://doi.org/10.1007/s00382-007-0252-y

Wang, W., Yang, K., Zhao, L., Zheng, Z., Lu, H., Mamtimin, A., et al. (2020). Characterizing surface albedo of shallow fresh snow and its importance for snow ablation on the interior of the Tibetan Plateau. *Journal of Hydrometeorology*, *21*(4), 815–827. https://doi.org/10.1175/JHM-D-19-0193.1

Wielicki, B. A., Wong, T., Loeb, N., Minnis, P., Priestley, K., & Kandel, R. (2005). Changes in earth's albedo measured by satellite. *Science*, *308*(5723), 825. https://doi.org/10.1126/science.1106484

Wu, G. X., Duan, A. M., Liu, Y. M., Mao, J., Ren, R., Bao, Q., et al. (2015). Tibetan Plateau climate dynamics: Recent research progress and outlook. *National Science Review*, *2*(1), 100–116. https://doi.org/10.1093/nsr/nwu045

Wu, G. X., Liu, Y. M., He, B., Bao, Q., & Wang, Z. Q. (2018). Review of the impact of the Tibetan Plateau sensible heat driven air-pump on the Asian summer monsoon. *Chinese Journal of Atmospheric Sciences*, *42*(3), 488–504. https://doi.org/10.3878/j.issn.1006-9895.1801.17279

Wu, G. X., Liu, Y. M., Zhang, Q., Duan, A., Wang, T., Wan, R., et al. (2007). The influence of mechanical and thermal forcing by the Tibetan Plateau on Asian climate. *Journal of Hydrometeorology*, *8*(4), 770–789. https://doi.org/10.1175/JHM609.1

Wu, T., & Qian, Z. (2003). The relation between the Tibetan winter snow and the Asian summer monsoon and rainfall: An observational investigation. *Journal of Climate*, *16*(12), 2038–2051. https://doi.org/10.1175/1520-0442(2003)016<2038:TRBTTW>2.0.CO;2

Xie, Z., Hu, Z., Ma, Y., Sun, G., Gu, L., Liu, S., et al. (2019). Modeling blowing snow over the Tibetan Plateau with the Community Land Model: Method and preliminary evaluation. *Journal of Geophysical Research: Atmospheres*, *124*(16), 9332–9355. https://doi.org/10.1029/2019JD030684

Yang, F., Mitchell, K., Hou, Y. T., Dai, Y., Zeng, X., Wang, Z., & Liang, X. Z. (2008). Dependence of land surface albedo on solar zenith angle: Observations and model parameterization. *Journal of Applied Meteorology and Climatology*, *47*(11), 2963–2982. https://doi.org/10.1175/2008JAMC1843.1

Yang, K., He, J., Tang, W. J., Lu, H., Qin, J., Chen, Y. Y., et al. (2019). China meteorological forcing dataset (1979–2018) [Dataset]. *A Big Earth Data Platform for Three Poles*. https://doi.org/10.11888/AtmosphericPhysics.tpe.249369.file

Yimin, L., Mengmeng, L., Haijun, Y., Anmin, D., Bian, H., Song, Y., et al. (2020). Land–atmosphere–ocean coupling associated with the Tibetan Plateau and its climate impacts. *National Science Review*, *7*(3), 534–552. https://doi.org/10.1093/nsr/nwaa011

Zhang, Q., & Huang, R. H. (2004). Parameters of land-surface processes for Gobi in north-west China. *Boundary-Layer Meteorology*, *110*, 471–478. https://doi.org/10.1023/B:BOUN.0000007224.08804.b8

Zhao, H., & Moore, G. W. K. (2004). On the relationship between Tibetan snow cover, the Tibetan plateau monsoon and the Indian summer monsoon. *Geophysical Research Letters*, *31*(14), 101–111. https://doi.org/10.1029/2004GL020040

Zhao, P., Zhou, Z., & Liu, J. (2007). Variability of Tibetan Spring snow and its associations with the hemispheric extratropical circulation and East Asian summer monsoon rainfall: An observational investigation. *Journal of Climate*, *20*(15), 3942–3955. https://doi.org/10.1175/JCLI4205.1

Zhao, Y., Li, Y. Q., Yang, X., He, D. Y., & Zhang, C. (2013). Impact of the Anomaly of Surface sensible heat in Qinghai-Xizang Plateau and its surrounding areas on summertime precipitation in Northern Xinjiang. *Plateau Meteorology*, *32*(5), 1215–1223. https://doi.org/10.7522/j.issn.1000-0534.2012.00117

Zheng, Z., Dong, W., Li, Z., Zhao, W., Hu, S., Yan, X., et al. (2015). Observational study of surface spectral radiation and corresponding albedo over Gobi, desert, and bare loess surfaces in northwestern China. *Journal of Geophysical Research: Atmospheres*, *120*(3), 883–896. https://doi.org/10.1002/2014JD022516

Zheng, Z., Wei, Z., Li, Z., Wei, H., & Liu, H. (2014). Study of parameterization of Surface Albedo of bare soil over the Gobi desert in the Dunhuang Region. *Chinese Journal of Atmospheric Sciences*, *38*(2), 297–308. https://doi.org/10.3878/j.issn.1006-9895.2013.13147

Zheng, Z., Wei, Z., Wen, Z., Dong, W., Li, Z., Wen, X., et al. (2017). Inclusion of solar elevation angle in land surface albedo parameterization over bare soil surface. *Journal of Advances in Modeling Earth Systems*, *9*(8), 3069–3081. https://doi.org/10.1002/2017MS001109

Zhou, W. Y., Guo, P. W., Luo, Y., Liou, K. N., Gu, Y., & Xue, Y. K. (2008). A study on the radiative transfer parameterization scheme within canopy in land surface process model. *Acta Meteorologica Sinica*, *66*(3), 359–370. https://dx.chinadoi.cn/10.3321/j.issn:0577-6619.2008.03.007

Zhou, X., Ding, B., Yang, K., Pan, J., Ma, X., Zhao, L., et al. (2023). Reducing the cold bias of the WRF model over the Tibetan Plateau by implementing a snow coverage-topography relationship and a fresh snow albedo scheme. *Journal of Advances in Modeling Earth Systems*, *15*(9), e2023MS003626. https://doi.org/10.1029/2023MS003626